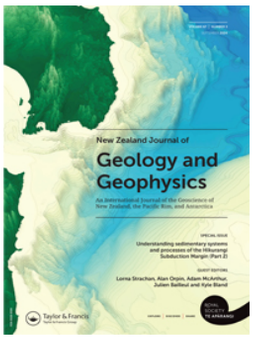

New Zealand Journal of Geology and Geophysics

ISSN: (Print) (Online) Journal homepage: www.tandfonline.com/journals/tnzg20

Integrating petrology, biogeochemistry, hyperspectral and thermal remote sensing for constraining the shallow hydrology of geothermal systems: Waiotapu Geothermal Field, Taupo Volcanic Zone, New Zealand

Cecilia Rodriguez-Gomez, Gabor Kereszturi, Robert Reeves & Andrew Rae

To cite this article: Cecilia Rodriguez-Gomez, Gabor Kereszturi, Robert Reeves & Andrew Rae (12 Jun 2024): Integrating petrology, biogeochemistry, hyperspectral and thermal remote sensing for constraining the shallow hydrology of geothermal systems: Waiotapu Geothermal Field, Taupo Volcanic Zone, New Zealand, New Zealand Journal of Geology and Geophysics, DOI: 10.1080/00288306.2024.2360032

To link to this article: https://doi.org/10.1080/00288306.2024.2360032

Published online: 12 Jun 2024.

NEW ZEALAND JOURNAL OF GEOLOGY AND GEOPHYSICS
https://doi.org/10.1080/00288306.2024.2360032

Taylor & Francis
Taylor & Francis Group

RESEARCH ARTICLE

OPEN ACCESS Check for updates

Integrating petrology, biogeochemistry, hyperspectral and thermal remote sensing for constraining the shallow hydrology of geothermal systems: Waiotapu Geothermal Field, Taupo Volcanic Zone, New Zealand

Cecilia Rodriguez-Gomez [a]*, Gabor Kereszturi[a], Robert Reeves[b] and Andrew Rae[b]

[a]School of Agriculture and Environment, Massey University, Palmerston North, New Zealand; [b]GNS Science, Wairakei Research Centre, Taupo, New Zealand

ABSTRACT

Studying geothermal areas can require significant resources, especially in areas densely covered by vegetation. This study integrates remote sensing techniques, including hyperspectral, thermal infrared and LiDAR with petrology and biogeochemistry of rock, soil and plant samples to develop a new shallow hydrogeological conceptual model of Waiotapu Geothermal Field, New Zealand. Previous studies present in detail each technique converging in this comprehensive research work. This geothermal area is densely covered by kanuka, an endemic shrub species to geothermal areas of New Zealand. Kanuka served as a key component in generating foliar element zonation maps for antimony and barium, utilising random forest classification validated by leave-one-out cross-validation. Thermal infrared data were employed to assess the behaviour of thermal anomalies through point pattern analysis. Results identified two intermingling processes within the single system: one in the north characterised by acid-sulphate alteration, bioavailability of barium to kanuka, and clustered surface thermal anomalies; another in the south where elements like silver, arsenic, and antimony are bioavailable to kanuka, accompanied by chloride-rich waters and denser yet non-clustered surface thermal anomalies. These cohesive methodology illustrates the efficacy of remote sensing techniques, showcasing the effectiveness of remote sensing in evaluating vegetated areas for geothermal exploration potential.

ARTICLE HISTORY
Received 28 December 2023
Accepted 29 April 2024

HANDLING EDITOR
Marshall Palmer

KEYWORDS
Airborne remote sensing; vegetation; Kanuka; acid sulphate; hydrothermal alteration; point pattern analysis; SWIR; thermal remote sensing

Introduction

Geothermal systems and their surface manifestations have played a critical role in human civilisation, initially as direct use for heating and cooking and evolving into a diversity of uses at present time (Jácome Paz et al. 2021; Lund et al. 2022). The latter includes electricity generation, cooling and heating spaces, and other industrial applications such as greenhouses, aquaculture and drying of wood (Lund et al. 2011; Barasa Kabeyi 2019; Soltani et al. 2019). Geothermal systems and their heat capacity depends on fluid temperature and composition, rock permeability, and tectonic setting (Pirajno 2009; Ciriaco et al. 2020; Mardiati et al. 2020; Renewable Energy Agency & Geothermal Association 2021), and these properties that can vary spatially and temporally (Lloyd 1959; Simpson and Christie 2019).

Geothermal systems that involve convection of hot fluids generally develop a series of mineral associations and surface manifestations from which subsurface activity can be inferred (Freski et al. 2021; Qudsi and Noor 2022). For example, acid sulphate alteration due to condensation of magmatic gases (e.g. H_2S, CO_2, SO_2) into groundwater can precipitate alunite, kaolin- and smectite-group minerals, and native sulphur, typically associated with springs, mud-pools and steam-gas vents (Aguilera et al. 2016; McCleskey et al. 2022; Montanaro et al. 2023). On the other hand, deep-sourced upflows discharging on the surface are often characterised by silica deposition forming sinter terraces and chloride-rich, near-neutral pools (Lynne 2012; Hamilton et al. 2019; Gong et al. 2022; Ünal Ercan et al. 2022). Alteration minerals related to neutral, deep waters include adularia, epidote, polymorphs of quartz, calcite and pyrite (Henley and Ellis 1983; Pirajno 2009).

Exploration and assessment of geothermal systems is done with a variety of methods, including geochemical (e.g. geothermometry, gas flux, isotopic analyses) (Wei et al. 2021; Jácome Paz et al. 2022; Pérez-Zárate et al. 2022), geological (e.g. lineament and mineral identification) (Mauriohooho et al. 2014; Calvin

CONTACT Cecilia Rodriguez-Gomez cecilia@eneryou.org; Gabor Kereszturi G.Kereszturi@massey.ac.nz
*Current affiliation: Eneryou, Tlalpan, 14268, México City, México

et al. 2015; Suherlina et al. 2022) and geophysical techniques (e.g. magneto-telluric, electrical, gravity, seismic and remote sensing) (Kellett and Bromley 2019; Hacıoğlu et al. 2021; Zhou 2021; Bertrand et al. 2022; Qudsi and Noor 2022). Some of these are surface techniques used to infer subsurface activity (e.g. geophysics, remote sensing, geological mapping), while others involve calculating parameters from the subsurface rock and fluids (e.g. magneto-tellurics, fluid chemistry). Some of these methods (e.g. magneto-tellurics, fluid chemistry, geological mapping) are expensive and/or time consuming, and most of these methods can be hindered by dense vegetation cover or steep topography. However, some remote sensing techniques, such as hyperspectral in the VNIR-SWIR region and single band Thermal Infrared (TIR), provide a functional methodology to perform the first steps of exploration and further monitoring of geothermal areas even in densely vegetated areas (Sun et al. 2022; Zaini et al. 2022; Rodriguez-Gomez et al. 2023a; Rodriguez-Gomez et al. 2023b).

This study presents an integrated model based on biogeochemistry, petrography and petrological observations, hyperspectral and thermal remote sensing analysis of the Waiotapu Geothermal Field (WGF), North Island of New Zealand, detail of each methodology step can be observed in Rodriguez-Gomez et al. (2023a, 2023b). WGF is an example of a natural laboratory, where novel methodologies and techniques can be tested for further use in similar intrusion-related geothermal systems hosted by volcanic rocks, such as geothermal systems of the Taupo Volcanic Zone (TVZ) (Rowland and Simmons 2012; Pope and Brown 2014). WGF is of particular interest due to its protected status since the 1980s which has prevented its large-scale exploitation (e.g. electricity generation), allowing for its natural evolution (Simpson and Bignall 2016). Therefore, the approach presented herein can provide an alternative for monitoring geothermal processes remotely without environmental harm, while further providing new insights into understanding of the shallow hydrology and geology of the WGF. The presented methodology also has the potential to be upscaled to monitor geothermal systems across the TVZ and beyond.

Geological setting

The WGF is located in the North Island of New Zealand, within the TVZ (Figure 1), with an overall orientation NNE-SSW resulting from an intra-arc continental rift between the Pacific and Australian Plates (Seebeck et al. 2014; Wilson and Rowland 2016). At WGF the basement rock, commonly referred to as 'greywacke', consists of a weakly metamorphosed Mesozoic sedimentary rock (Hedenquist 1991; Milicich

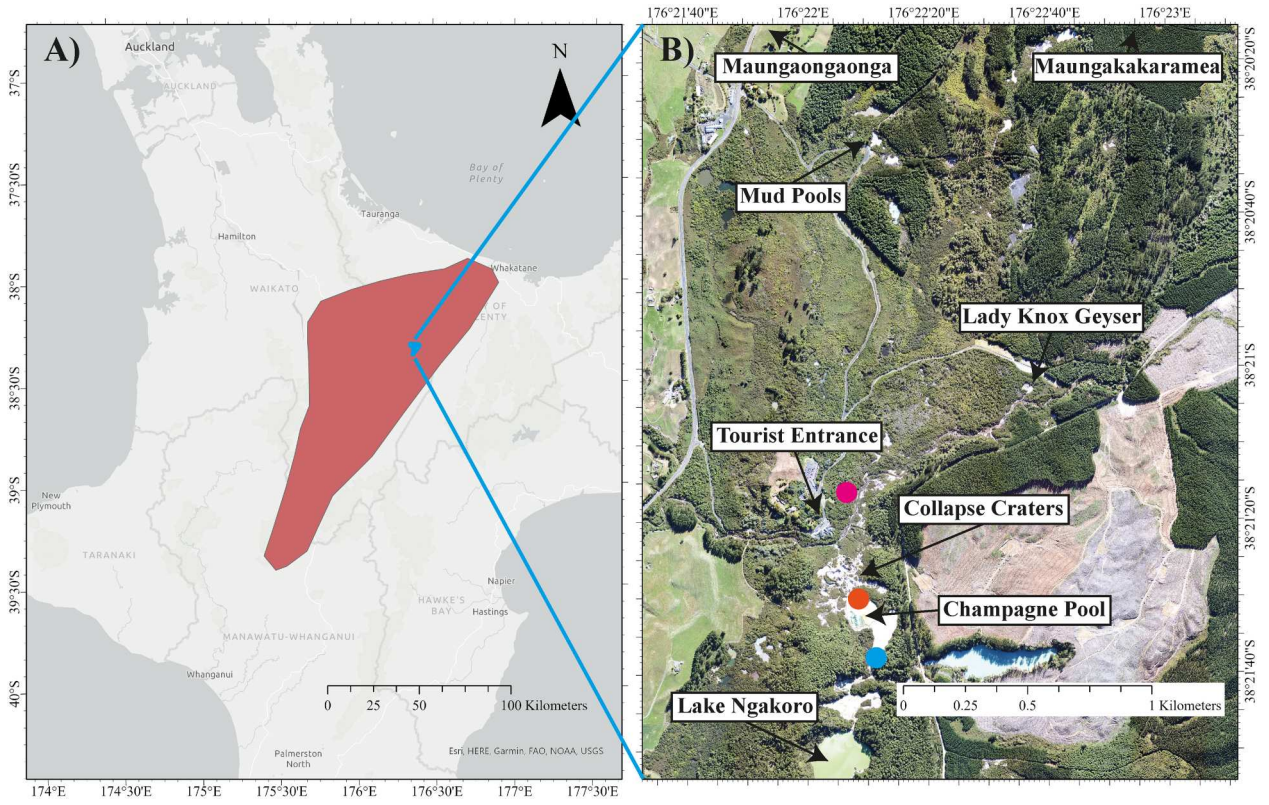

Figure 1. A, Location of WGF (represented by blue polygon) within the TVZ (represented by red polygon). B, Close-up to WGF (blue polygon in 1.A) depicted by blue lines. WGF on a true-coloured orthophoto. Geographic locations mentioned in the text are labelled in figure. Coloured circles correspond to WAI_06 (pink), WAI_22 (orange) and WAI_27 (blue) samples shown on Figure 3, respectively.

et al. 2020). The basement is overlain by predominantly rhyolitic volcanic and volcanoclastic deposits sporadically intercalated by lacustrine sediments (Steiner 1963; Grindley et al. 1994), like the Huka Falls Formation (Cattell et al. 2016). The latter is a clay-rich mudstone and siltstone formation that is a spatially discontinuous litho-cap layer for many of the TVZ geothermal systems (Lloyd 1959; Wood 1994).

Similar to other hydrothermal systems in volcanic settings, WGF hosts a wide variety of surface manifestations including mud-pools, fumaroles, geysers, chloride-rich pools and silica sinter terraces (Lloyd 1959; Hedenquist and Browne 1989) (Figure 2). The heat source has been located at the north of the system near Mounts Maungaongaonga and Maungakakaramea (Figure 1) (Rowland and Sibson 2004). The conceptual model has a chloride-rich fluid reservoir located at 1–4 km depth at a temperature >250°C that is based on borehole geology, numerical modelling and geochemical studies (Steiner 1963; Hedenquist 1991; Giggenbach et al. 1994; Kaya et al. 2014, 2015). The heated high-chloride fluids reach the surface at 75°C at the south of the geothermal system, after migrating horizontally along <50 m topographic change (Hedenquist 1982; Giggenbach 1995; Kaya et al. 2014). The horizontal fluid flow has been postulated to be due to high intrinsic horizontal permeability of the Waiotapu Ignimbrite (Mongillo 1994; Wood 1994; Hadfield et al. 2001; Kaya et al. 2015).

Acid-sulphate alteration with mineral associations of kaolinite, alunite, native sulphur, cristobalite and fine grained pyrite is prevalent throughout the WGF at various depths (Hedenquist and Browne 1989; Hedenquist 1991; Rodriguez-Gomez et al. 2021), however, these mostly occur in northern areas (Figure 2A, B). On the contrary, towards the south, the WGF presents intermingled alteration mineralogy including albite/adularia/chlorite/epidote at depth, and recrystallised groundmass rich in quartz polymorphs at various depths (Hedenquist and Browne 1989) (Figure 3). The discontinuous litho-cap facilitates the formation of patches of mixed sulphate–chloride mineralisation, including phyllosilicate minerals, native sulphur and silica polymorphs (Hedenquist 1982; Hedenquist and Browne 1989; Rowland and Simmons 2012; Kaya et al. 2014). Furthermore, changes in water table levels, erosion and ground movement have provoked surface shifts of sinter depositing springs. These changes occur at water table level, occasionally causing hydrothermal eruptions, with mineral alteration causing the weakening of the rock provoking collapse craters (Figure 2D) (Lloyd 1959; Hedenquist and Browne 1989; Gallagher et al. 2020).

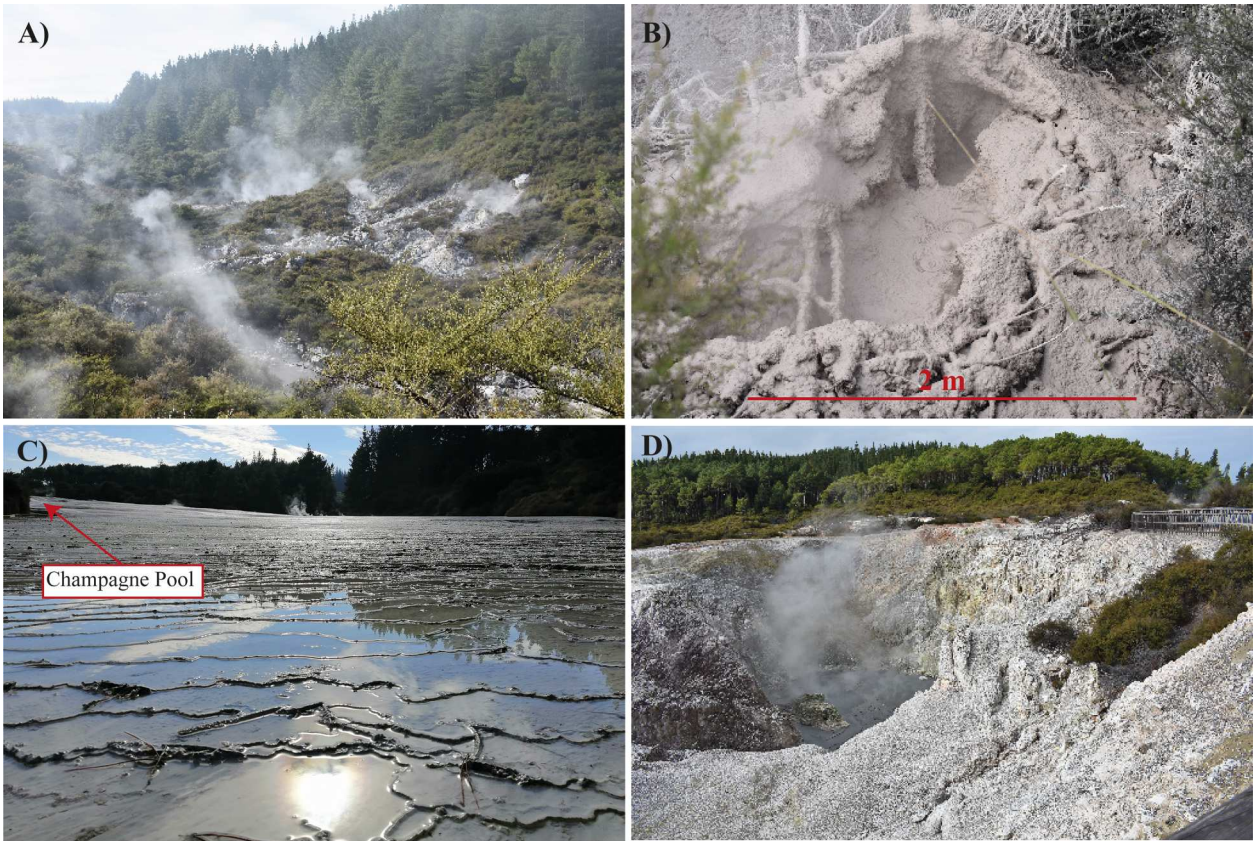

Figure 2. Geothermal surface features at WGF. A, Steaming grounds with dense vegetation cover of Kanuka and Pinus radiata plantations in the background. B, Mud pool occurring on the northern areas of WGF. C, Silica sinter depositions in terraces, from overflowing waters of Champagne Pool's chloride-rich waters. D, Collapse craters with active steaming.

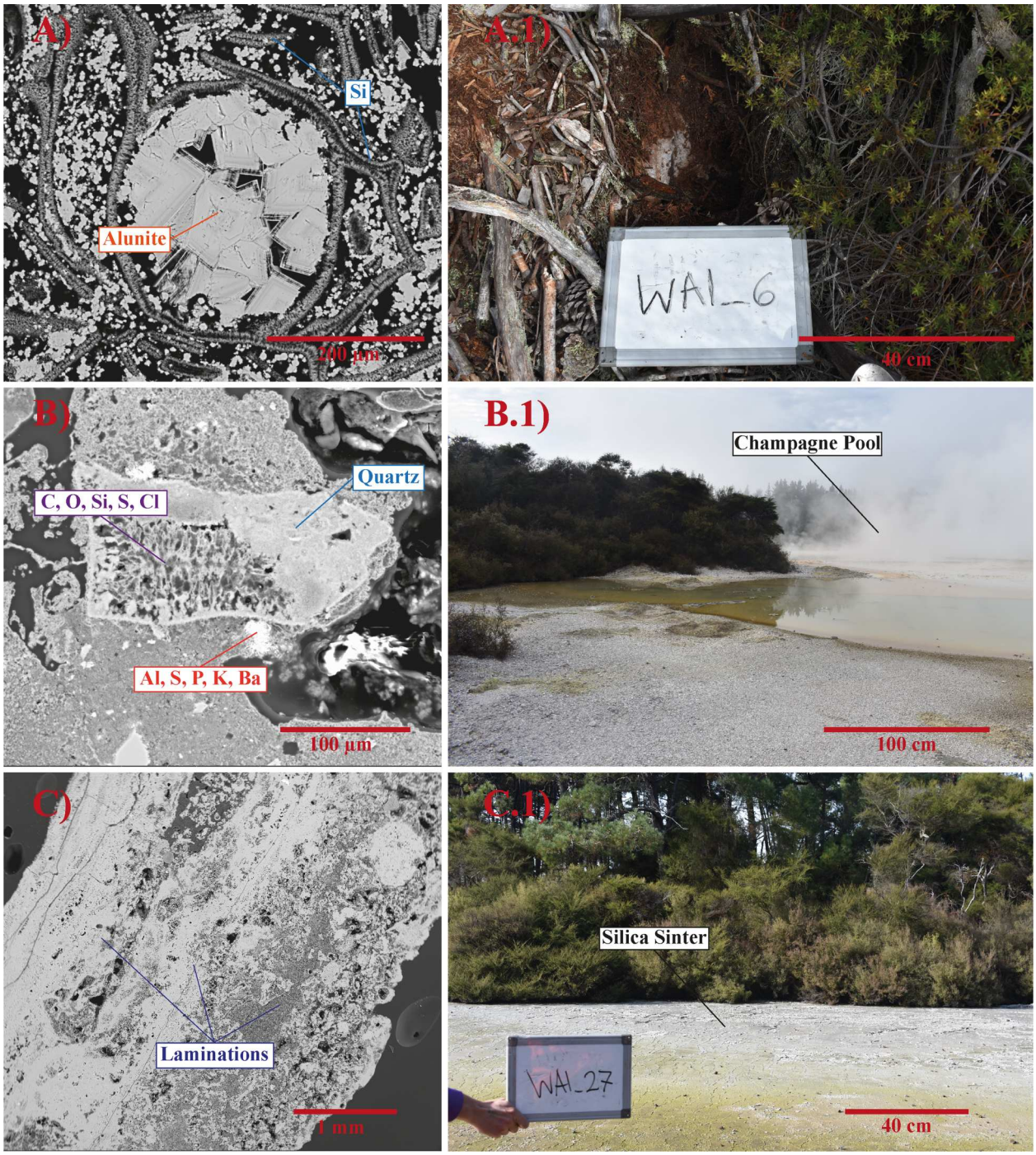

Figure 3. SEM photos for three rock samples and their respective sampling site. A, Sample WAI_06 shows alunite precipitation inside voids with crystallised silica walls. Sample WAI_06 was taken from the northern area of the system (Figure 1B, pink circle). B, WAI_22 shows mineralisation of quartz polymorphs, along with biotic and abiotic enrichment of C, Si, S, Cl elements. Presence of Al, S, P, K and Ba was detected within the matrix. Sample WAI_22 is from the vicinity of Champagne Pool (Figure 1(B), orange circle). C, WAI_27 shows laminated silica sinter deposits mixed with biological matter near the outflow of Champagne Pool. This sample was taken from the silica sinter terraces, south of Champagne Pool (Figure 1B, blue circle).

The natural vegetation cover at WGF is dominated by *kunzea ericoides* var. *microflora* also known as 'kanuka' an endemic species to geothermal areas of New Zealand (Figure 4) (Given 1980; Deroin et al. 1995; Smale et al. 2018). Kanuka, also known as white tea tree, is a spreading shrub with white or pink flowers, extremely tolerant of acidic soils and ground temperatures >40°C (Mia et al. 2012; Smale and Fitzgerald 2015; Beadel et al. 2018). Vegetation cover can be perceived as a limitation to exploration techniques, however, previous studies have used it to assess ground heat changes in combination with other datasets in a qualitative manner (Elmarsdóttir et al. 2015; Seward et al. 2022), and monitor the effects of geothermal energy exploitation (Lattanzi et al. 2020). Therefore, vegetation can provide key information about the shallow subsurface as it can dynamically react to geothermal activity: soil and

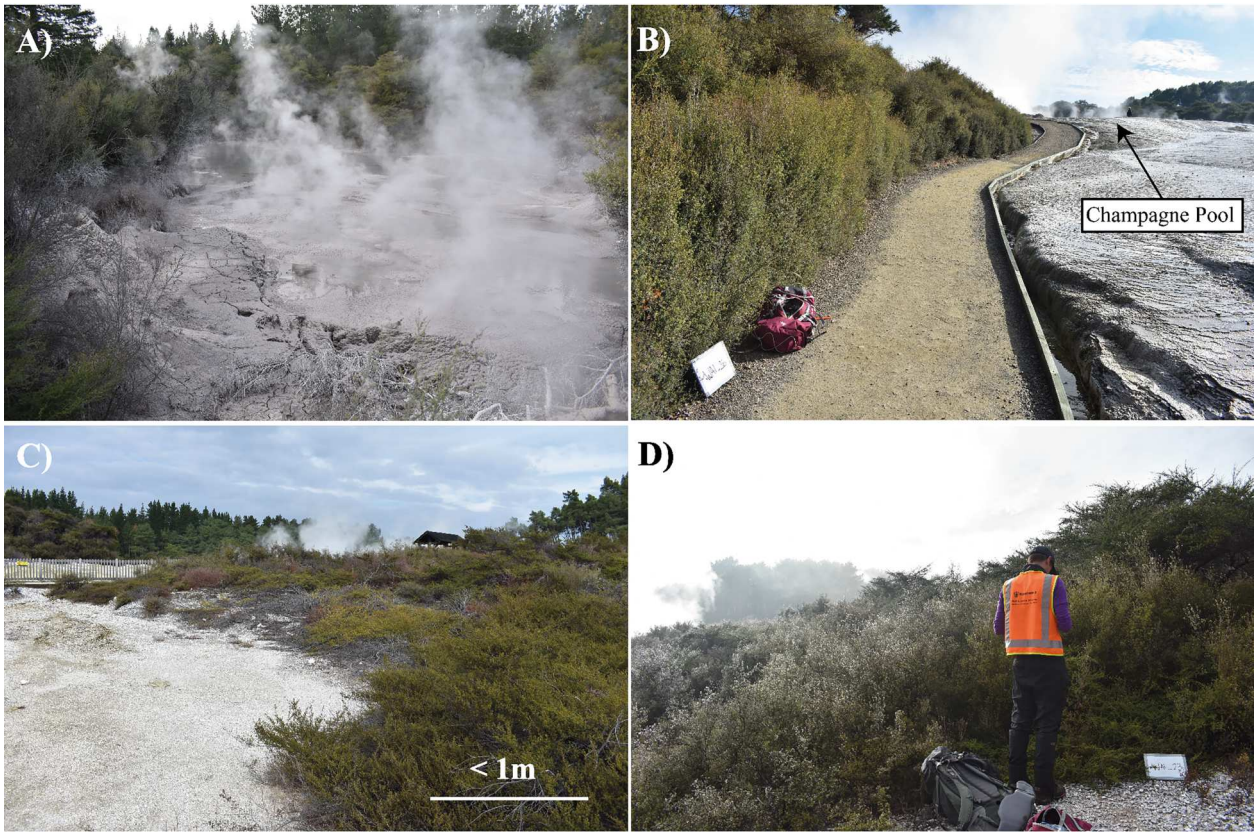

Figure 4. Field photos exhibiting different styles of growth for Kanuka shrub. A, Kanuka next to mud-pools in the northern area of the system where acid-sulphate alteration is prevalent. B, Kanuka shrub next to silica sinter terraces. C, Kanuka growing short and close to the ground (<1 m tall), also known as 'prostrate' kanuka, provides an indicator of hotter ground temperatures. D, Tall kanuka plants living in colder ground areas (~20°C), reaching heights of 2 m or more.

water chemistry, geothermal heat and gas emissions and nutrient availability (Mia et al. 2012; Van Manen and Reeves 2012).

Materials and methods

WGF is an area which has been explored for decades with a variety of geophysical, geological and geochemical techniques. With the advancement in remote sensing techniques a new wave of exploration techniques has arisen, providing an opportunity to re-explore areas from a different perspective. Here, we used a combination of airborne hyperspectral and thermal data complemented with rock, soil and plant samples to revise the conceptual model of WGF. Rock was sampled where available and soil was sampled in all the sampling sites. In this document we present the convergence and interpretations of a broader study which involves previous publications, for deeper analysis on each section of the methodology, please refer to Rodriguez-Gomez et al. (2023a, 2023b)

The 77 rock and soil samples along with the 77 kanuka foliage samples were collected from WGF a week after the aerial hyperspectral and TIR surveys (Rodriguez-Gomez et al. 2023a). The rock and soil samples were air dried and subjected to Scanning Electron Microscopy and Shortwave Infrared Reflectance Spectroscopy at Massey University, New Zealand to constrain their mineralogy and petrology. The plant samples were dried, ground and sieved to be analysed with an ICP-MS for 53 elements at Acme Labs – Bureau Veritas, Canada. Find more information and detail about sample preparation for chemical concentration analyses in Rodriguez-Gomez et al. (2023a).

Airborne-based hyperspectral data were collected with an AisaFENIX sensor (Pullanagari et al. 2016), covering visible near infrared (VNIR) to shortwave infrared (SWIR) ranges between 370 and 2500 nm with 3–7 nm spectral sampling interval. The hyperspectral data were subjected to radiometric and atmospheric correction, followed by georectification using ground control points, following Kereszturi et al. (2020). The airborne hyperspectral data were then used in combination with the foliar ICPMS data to develop new elemental concentration zonation maps using random forest classifications (for details see Rodriguez-Gomez et al. 2023a). The random forest classifications were developed for barium and antimony, that were validated via leave one out cross-validation.

Thermal infrared data were acquired with a FLIR A615 sensor ranging between 7500 and 13,000 nm, only 10 h after the hyperspectral data, and it was calibrated against water body temperatures measured in

sync with the airborne survey (details in Reeves and Sanders 2019). Thermal anomalies were delineated as >13°C (i.e. ambient temperature), and filtered before subjected to point pattern analysis (see details in Rodriguez-Gomez et al. 2023b). The LiDAR data were obtained from Land Information New Zealand (LINZ) Data Services and vegetation height was obtained by subtracting the Digital Surface Model from the Digital Elevation Map.

These analytics returned (1) foliar elemental zonation maps as a proxy for subsurface lithology, alteration and fluid composition, and (2) distribution of thermal anomalies. The integration of such new datasets (Figure 5) allows us to better understand the shallow fluid flow and geology of the WGF in present time.

A unified geological model for Waiotapu Geothermal Field

The chloride-rich parental fluid at WGF estimated to be at a depth of 1–4 km based on drill core information and numerical models, is heated to ~270°C by a magmatic source located at the north of the system (Hedenquist and Browne 1989; Giggenbach et al. 1994; Kaya et al. 2014). After a vertical ascent, the parental fluids move laterally and discharge at the surface about 4 km to the south principally at Champagne Pool (Figure 1). The lateral water and heat transport is due to high horizontal permeability of the rhyolitic ignimbrite host rock (Hedenquist 1991; Kaya et al. 2014). Furthermore, the lateral fluid flow creates changing heat output styles which have been detected thermally with the TIR imagery and point pattern analysis (Figure 6). The north presents thermal anomaly clusters separated by 250 m, and low density of thermal anomalies (i.e. 396 thermal anomalies per km^2), while no clustering and higher density of thermal anomalies (i.e. ~7000 thermal anomalies per km^2) are observed in the south (Figure 6) (Rodriguez-Gomez et al. 2023a). The measured separation of 250 m, could be an indicator of cell convection forming permeable pathways through the litho-cap (e.g. McLellan et al. 2010; Patterson et al. 2018). Overall, the observed thermal anomalies also align with the regional tectonics (i.e. Paeroa and Ngapouri Faults), with a strike of ~ N22E° (Grindley et al. 1994; Wilson and Rowland 2016).

The proposed lateral flow and changing heat output style have further been imprinted into the kanuka-dominated vegetation cover that show: changing canopy height, foliar chemistry and canopy reflectance properties (Rodriguez-Gomez et al. 2023a). Elements such as silver (Ag), arsenic (As), and antimony (Sb) are transported to surface by the deep parental fluids and translocated by kanuka due to their bioavailability in liquid form (Ballantyne and Moore 1988; Tschan et al. 2009; S. C. Wilson et al. 2010). These elements have been documented to cause stress to plants via degradation of foliar pigments (Sanches et al. 2013), which is in turn detectable in their spectral reflectance

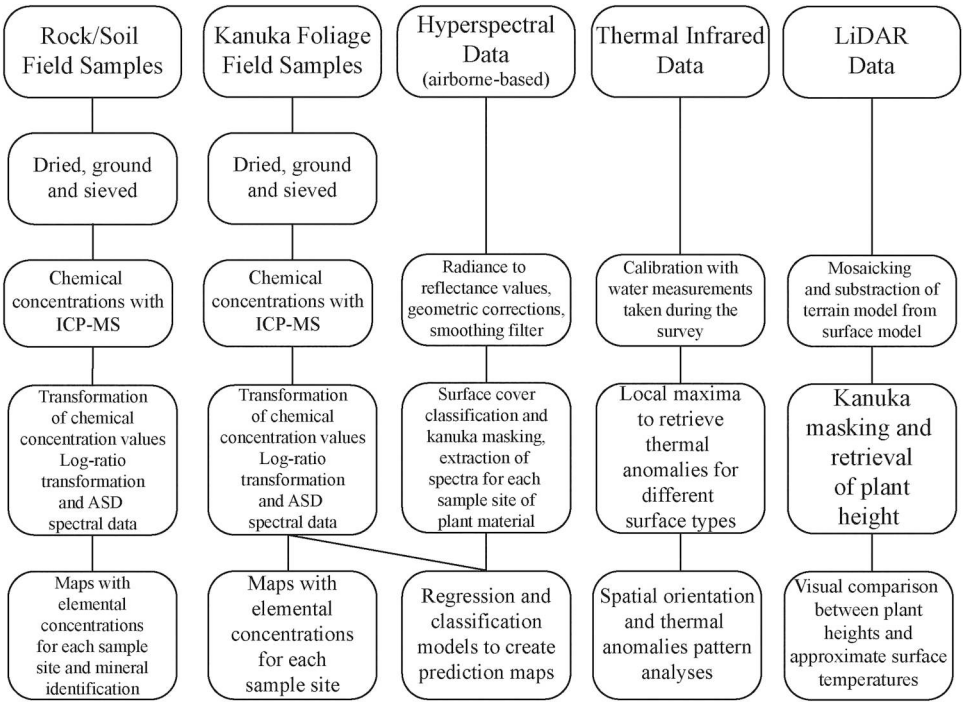

Figure 5. The flowchart shows the novel combination of methods employed for geothermal exploration at WGF, based on field samples including rock, soil and foliage samples, hyperspectral, thermal infrared and LiDAR data. Kanuka was the only species analysed both in field samples and in the spectral data after classification of plant species and selection of only kanuka to create a 'kanuka masking' layer. More detail on rock, soil and foliage preparation for chemical concentrations in ICP-MS can be found in (Rodriguez-Gomez et al. 2023a).

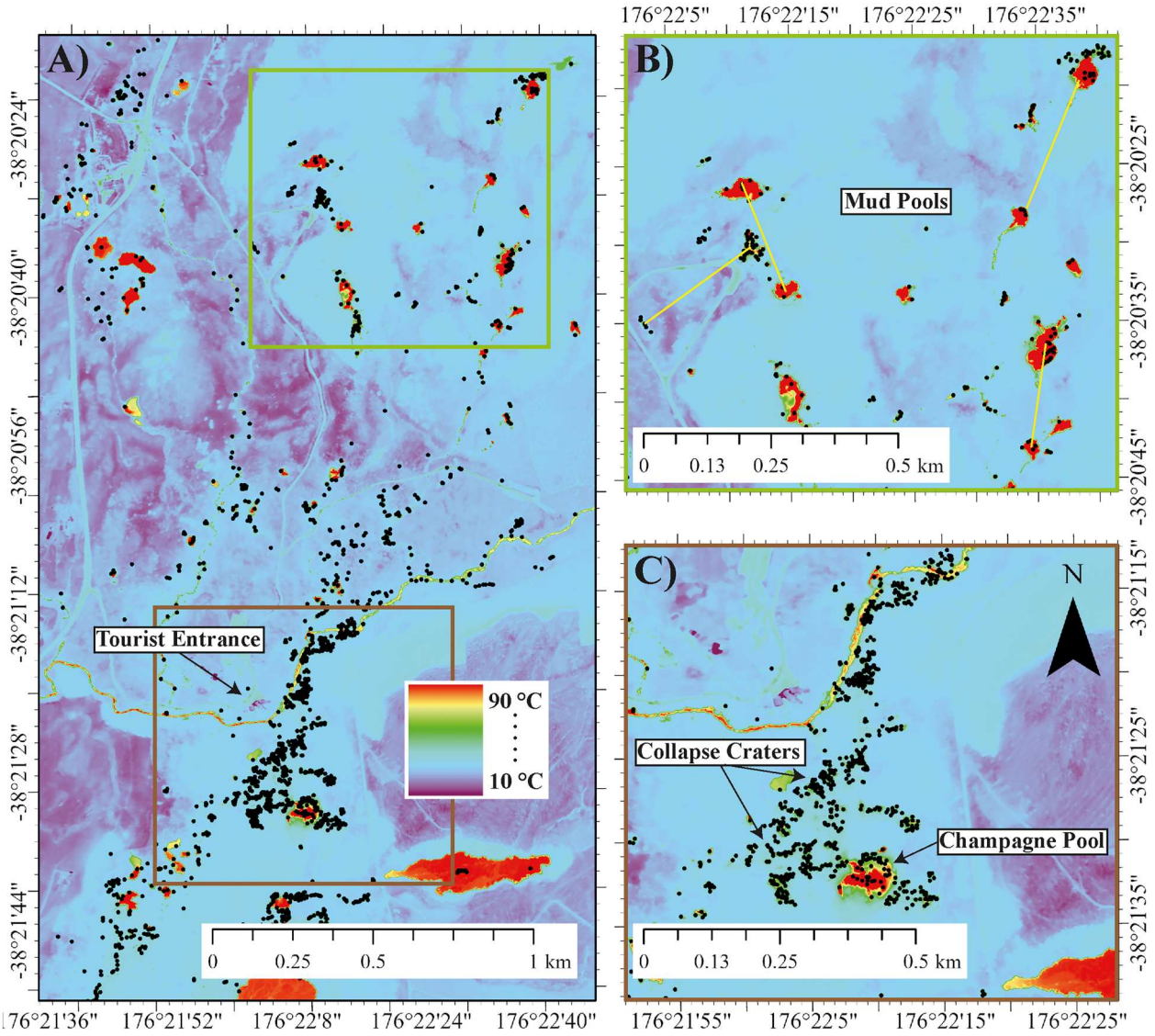

Figure 6. A, TIR image of WGF overlaid by filtered thermal anomalies as black dots. B, TIR image close-up of mud pools in the northern area of WGF, overlaid by thermal anomalies as black dots and yellow lines representing 250 m of separation between thermal anomaly clusters. Area shown in Figure 6A as a green square. C, TIR image overlaid by thermal anomalies in the sulphate-chloride zone and Champagne Pool, higher density of thermal anomalies can be observed. Area shown in Figure 6A as a brown square.

within the VNIR-SWIR (Finnegan and Chen 2012; Rathod et al. 2018; Rodriguez-Gomez et al. 2023a). In contrary, further away from the chloride-rich surface features like Champagne Pool, barium (Ba) becomes bioavailable in the periphery of the system where hot geothermal waters mix with cold groundwater (Dunn 2007). Ba has been documented to cause metal-induced stress in *Pteris* Ferns plants, which can be detected via reflectance spectroscopy (Slonecker et al. 2009).

Chloride-rich surface discharge is concentrated and in its most undiluted form at the Champagne Pool, where it flows mostly towards the south to form silica sinter terraces (Figure 2C). The uprising chloride-rich fluids are diluted by discontinuous H_2S and CO_2-rich steam-heated waters, indicated by the measured wide range of chloride concentration (200–1800 mg/kg) (Lloyd 1959) at hot springs. Further, strong elemental enrichment in Ag (0.01–6.9 mg/kg), As (0.7–12,000 mg/kg), Au (0.001–3.3 mg/kg), and Sb (0.02–392 mg/kg) as has been reported from water chemistry surveys (Lloyd 1959; Giggenbach et al. 1994). Within this area there is a mixing zone between chloride-rich and sulphate-rich, this zone where alteration 'endmembers' intermingle, is also indicated by a change in thermal anomaly point pattern, with a diffuse style of heat output and no clustering between thermal anomalies (Rodriguez-Gomez et al. 2023b), which can be interpreted as a combination of a thinning litho-cap towards the south (Wood 1994) and an increase in the host rock's permeability, due to weakening of the rock via hydrothermal alteration and/or frequent hydrothermal eruptions (Hedenquist and Browne 1989; Kaya et al. 2015; Simpson and Bignall 2016). Ground mineralogy in this mixing area presents a range of silica polymorphs,

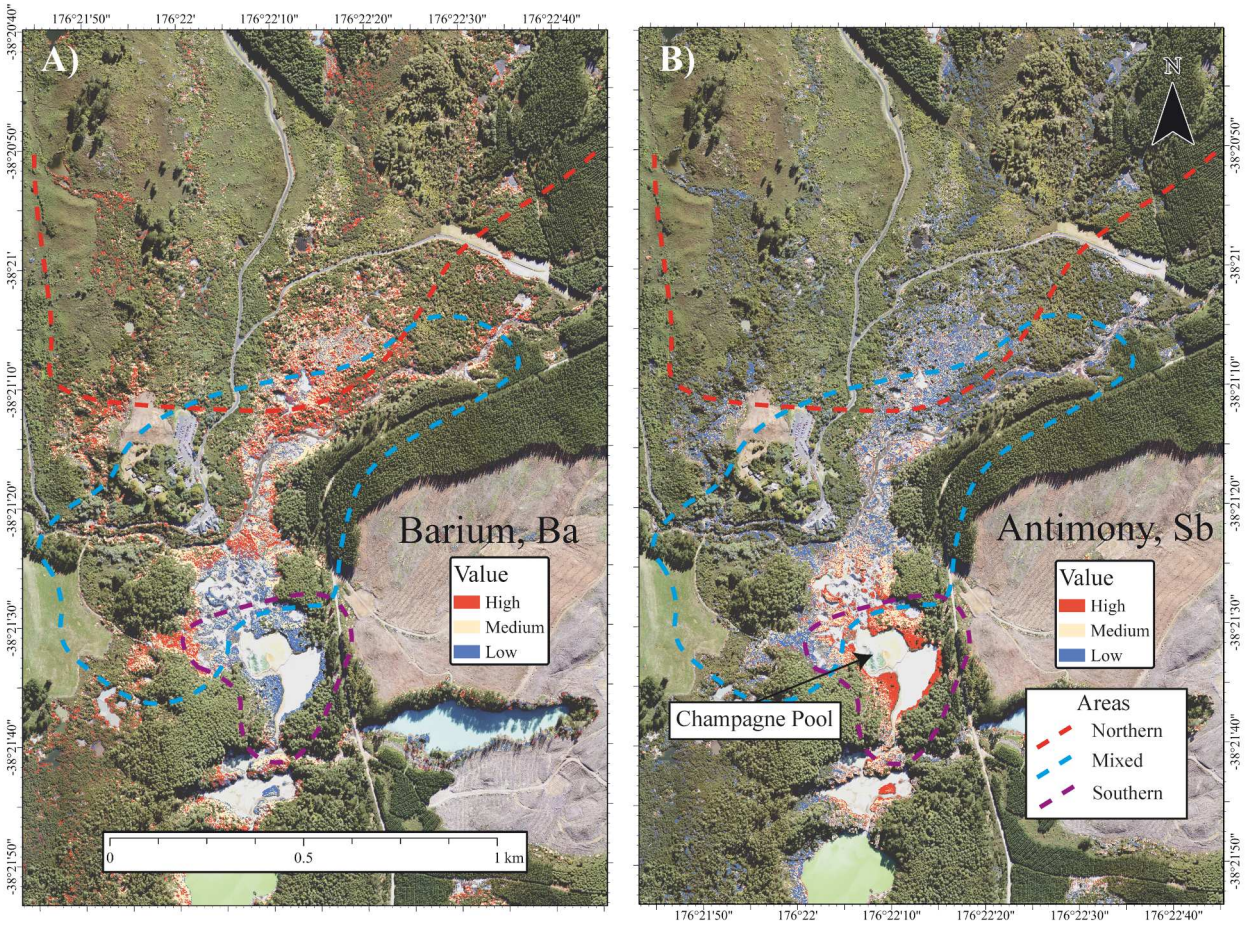

Figure 7. Zonation maps for Ba and Sb elements in kanuka foliage, with high, medium and low ranges. A, WGF on a true-coloured orthophoto, overlaid by the element zonation for Ba. B, WGF on a true-coloured orthophoto, overlaid by the element zonation for Sb.

phyllosilicate minerals and precipitation of native sulphur (Rodriguez-Gomez et al. 2021). Furthermore, in this area kanuka growth is hindered, with shallow roots and heights typically below 1 m (Figure 4C) (Boothroyd 2009; Rodriguez-Gomez et al. 2023a).

Furthermore, remotely sensed foliar concentration maps indicate similar concentric pattern of elements (e.g. Ag, As, Sb in Figure 7) in proximity to Champagne Pool (Rodriguez-Gomez et al. 2023a), indicating strong discharge of such elements into the shallow proportion of the geothermal system. In this region element enrichment of Sb has been described for kanuka plants (Dunn 2007; Dunn and Christie 2020), along with Ag and As that has been shown in (Rodriguez-Gomez et al. 2023a). Ba is enriched in rock and soil samples throughout the system, but only present in kanuka foliage in areas with low pH (Figure 7A). The prediction maps of Ba and Sb (Figure 7) represent a clear zonation of such indicator elements within the WGF. The elemental concentration of Ag, As and Sb increase (Figure 7; Rodriguez-Gomez et al. 2023a) in proximity to chloride-rich surface features (e.g. Champagne Pool). Further away from the discharge zone, such elements decrease sharply in both rock, soil and plant foliage while Ba shows enrichment in foliage (Figure 8) (Rodriguez-Gomez et al. 2023a). However, while Ba is present throughout the WGF in substrate (e.g. Figure 6 in Rodriguez-Gomez et al. 2021), it only becomes bioavailable where mixing of hot geothermal waters with cold groundwater takes place, such as the periphery of geothermal systems (Dunn 2007; Bundschuh and Maity 2015). This occurs because Ba increases its solubility with decreasing pH and reacts into an insoluble salt in waters with high sulphate content (Figures 7 and 8) (Brumbaugh et al. 2011; Monteiro et al. 2011; Sleimi et al. 2021).

The new hyperspectral foliar chemistry and thermal remote sensing data indicates current activity (i.e. a geological snapshot) of WGF (Figure 8) and can provide new tools for monitoring geothermal environments. However, we acknowledge the inherent dynamic nature of geothermal systems, which can only be resolved with repeated surveys and integration of other geophysical and geochemical methods. Combination of methods can also account for the possible translocation of elements from relic mineralisation and not present activity. Furthermore, the study of vegetation, particularly of kanuka in New Zealand, presents new opportunities to complement

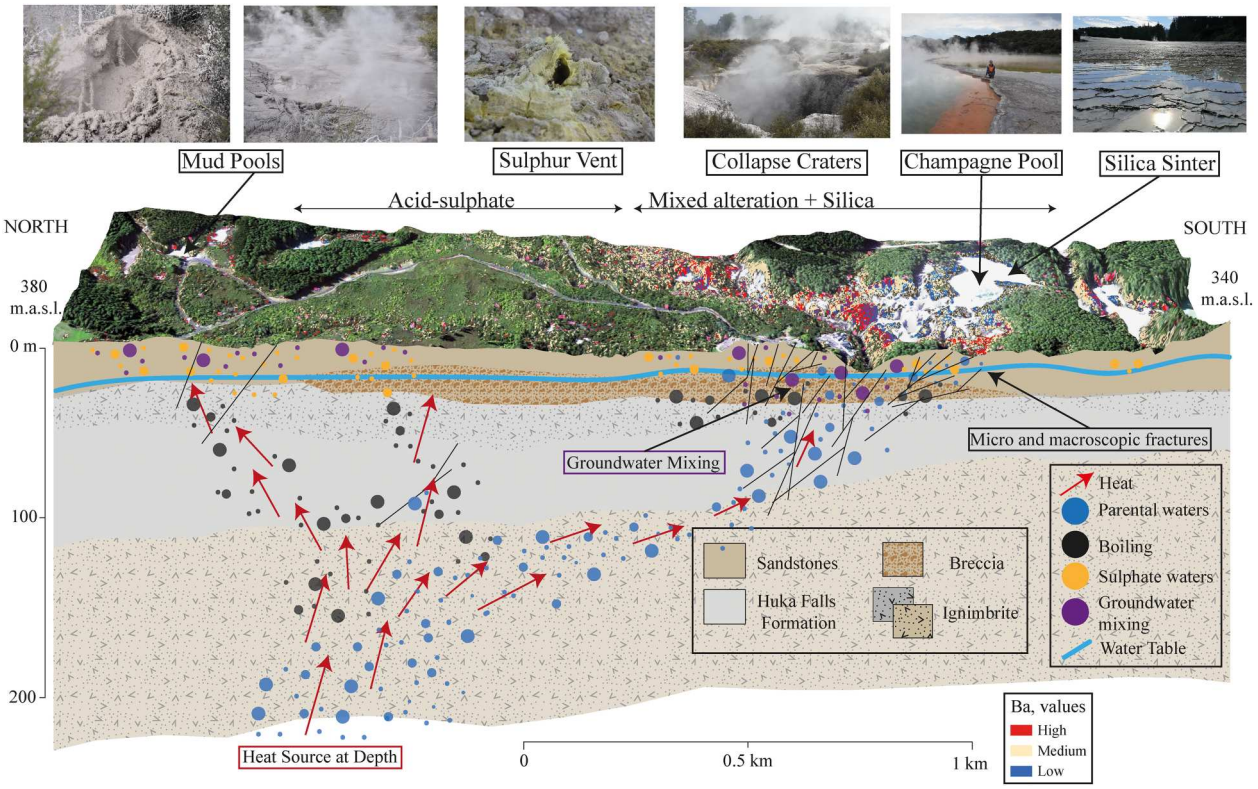

Figure 8. WGF cross section representing a unified geological model. The hot chloride-rich fluid rises, boiling and altering the host rock to form acid-sulphate surface features in the north while in the southern areas the chloride-rich parental waters emerge to surface in Champagne Pool and its surroundings. The WGF surface is presented on a true-coloured orthophoto, overlaid by Ba element zonation map. Field photos presented on top. X and Y axis have different scales.

monitoring surveys and first studies of geothermal areas in an efficient and novel manner.

Implications for geothermal exploration

Only 9 out of 29 high temperature geothermal fields in New Zealand are presently utilised for power generation (Simpson and Bignall 2016). WGF, recognised by the regional council as 'Waikite-Waiotapu-Waimangu' along with another 5 geothermal fields (Orakei Korako, Te Kopia, Horomatangi, Tongariro and Ruapehu), have a 'Protected' status and therefore will not have large-scale geothermal development. However, geothermal exploration in New Zealand has been active since the 1950s, with Wairakei becoming the first operational power plant in 1958, starting with a generation of 11.2 MWe (Lund et al. 2022), and the country is in the path of decarbonisation.

Most high-temperature geothermal systems in the TVZ share many commonalities. For example, they have rhyolitic volcanic sequences overlying metasedimentary basement rocks, have liquid dominated reservoirs and are fed by near-neutral chloride-rich waters. They also form similar geothermal features on the surface, including geysers, steaming ground, silica sinters, mud pools, fumaroles and sulphur mounds (Simpson and Bignall 2016). Furthermore, most of the geothermal systems in New Zealand also share similar mineralogy/alteration styles and permeability structures (Wilson and Rowland 2016; Bertrand et al. 2022), as well as plant communities (e.g. kanuka, ferns, lichens, moss) (Burns 1997; Beadel et al. 2018). Hence, WGF can be considered a representative geothermal field, where similar workflows could be expanded to other TVZ geothermal systems to monitor their shallow hydrology.

The potential of kanuka shrub for measuring foliar element concentration lies in its capability to translocate metals and metalloid that interfere with their metabolism and, hence impacting their spectral reflectance. This has also been reported for *Pinus Radiata* around gold deposits (Chakraborty et al. 2021) and pot-based experiments using *Brassica rapa chinesis* and *Rubus fruticosus* L. (Wang et al. 2018; Lassalle et al. 2019). This concept can be detected indirectly using hyperspectral remote sensing which allows for the underlying geochemical and geological processes in geothermal areas of New Zealand to be inferred. Combining the hyperspectral imagery with ground-based samples, the developed foliar element maps (Figure 7) mimic well with underlying hydrology and overall lithology type (e.g. known from drill cores, water chemistry and other geological/geophysical mapping) (Figure 8) (Rodriguez-Gomez et al. 2023a). However, tandem sampling soil/host rock is

also recommended to elucidate element mobility and bioavailability processes which could vary between different geothermal areas (e.g. Van Manen and Reeves 2012; Pullagurala et al. 2018; Rodriguez-Gomez et al. 2023a). Other plant species living in the vicinity of geothermal areas should also be sampled and analysed to further understand the translocation processes for each species (Dunn et al. 2018).

The point pattern analysis using TIR imagery (Figure 6) can be a time and cost-effective method (Harvey and Luketina 2014; Abubakar et al. 2019), for analysing heat-output in geothermal systems of New Zealand (Mongillo 1994; Mia et al. 2012; Harvey et al. 2016; Reeves and Sanders 2019). This method could be applied as a time-series analysis with repeat surveys, which can make it appropriate for monitoring purposes, assessing and understanding spatio-temporal heat associations within the system, particularly in the shallow subsurface (<200 m) (Rodriguez-Gomez et al. 2023a). Furthermore, the high spatial resolution which airborne and drone TIR surveys can provide, could be employed to monitor hazards in geothermal areas (e.g. Hipaua landslide, Tokaanu, New Zealand) (Hegan et al. 2001).

Internationally, countries located in template temperatures with tropical climates such as México, Dominica, Indonesia and Costa Rica have geothermal systems densely covered by vegetation, and therefore these exploration methods can aid in such contexts. Plant species that are thermotolerant and prevail in the harsh environment of geothermal areas have already been identified, including shrubs in Italy (*Evernia prunastri, Calluna vulgaris*), sagebrush in USA (*Artemisia tridentata*), shrubs in Kenya (*Tarchonanthus camphoratus*) or grasses in Mexico (*Allenrolfea occidentalis* and *Thypa dominguensis*) (Way and Hall 2001; Nash et al. 2003; Manzo et al. 2013; Pippucci et al. 2015; González-Acevedo et al. 2018; Lattanzi et al. 2020). Species like these ones can therefore become a primary target for geothermal exploration efforts with hyperspectral imaging, opening up new avenues for development and use of technology for understanding and exploring geothermal resources.

Conclusions

WGF can be sub-divided broadly into spatial zones that are characterised by an array of physical and chemical properties. The northern part is characterised by acid-sulphate alteration, the south by chloride-rich surface features which intermingle with an intermittent sulphate-rich layer which creates a third mixed zone (Hedenquist and Browne 1989; White and Hedenquist 1990; Rodriguez-Gomez et al. 2021; Rodriguez-Gomez et al. 2023a). These zones present different heat output styles, element enrichment and bioavailability, which were detected through remote sensing techniques (e.g. hyperspectral, TIR and LiDAR) (Rodriguez-Gomez et al. 2023a, 2023b) and interpreted in conjunction with previous studies of WGF. Mainly observing surface lithology type, vegetation spectral response and point pattern of thermal anomalies.

The presented methods can be improved by a larger number of field samples (e.g. Rattenbury et al. 2018; Santaga et al. 2021), covering a diverse range of locations (e.g. temperature, type of lithology, elevation, closeness to surface features) as well as background values that are located outside of the geothermal field. Due to the complexity of geothermal environments a deeper understanding of how fluid chemistry, soil pH and temperature affect plants is required. Controlled experiments with the species of interest (e.g. indicator species or metal accumulators) should be carried out to understand each parameter individually and as a group, to observe how this is reflected in its spectral signature.

WGF is a great natural laboratory to develop new methods that are non-invasive and benefit from a variety of surface features. The methods and workflows presented can open a window of opportunities for time and cost-effective techniques to be applied for the exploration and monitoring of geothermal areas with dense plant cover in New Zealand and other parts of the world, enabling the utilisation of geothermal resources worldwide.

Acknowledgements

The authors are grateful for the support and permits granted by Ngati Tahu – Ngati Whaoa Runanga Trustees (40/2015), Timberlands Limited and the Department of Conservation (78428-GEO). Hyperceptions/Aero-Works Ltd are thanked for the hyperspectral airborne-based image acquisition, and Specim Ltd. for the support in image processing. GNS Science provided the thermal infrared imagery. LiDAR data were downloaded from Land Information New Zealand's website (https://www.linz.govt.nz/ data/linz-data-service). Finally, the authors thank Colin Dunn at Colin Dunn Consulting Inc at Acme Labs – Bureau Veritas, Vancouver, Canada, for the chemical concentration analyses.

Disclosure statement

No potential conflict of interest was reported by the author(s).

Funding

This work was supported by Royal Society Te Apārangi [Catalyst Fund, CSG MAU1705].

Data availability statement

The data that support the findings of this study are available from the corresponding author, CRG, upon reasonable request.

ORCID

Cecilia Rodriguez-Gomez http://orcid.org/0000-0002-0211-1201

References

Abubakar AJ, Hashim M, Pour AB. 2019. Remote sensing satellite imagery for prospecting geothermal systems in an aseismic geologic setting: Yankari Park, Nigeria. International Journal of Applied Earth Observation and Geoinformation. 80(April):157–172. doi:10.1016/j.jag.2019.04.005.

Aguilera F, Layana S, Rodríguez-Díaz A, González C, Cortés J, Inostroza M. 2016. Hydrothermal alteration, fumarolic deposits and fluids from Lastarria Volcanic Complex: a multidisciplinary study. Andean Geology. 43(2):166–196. doi:10.5027/andgeoV43n2-a02.

Ballantyne JM, Moore JN. 1988. Arsenic geochemistry in geothermal systems. Geochimica et Cosmochimica Acta. 52(2):475–483. doi:10.1016/0016-7037(88)90102-0.

Barasa Kabeyi MJ. 2019. Geothermal electricity generation, challenges, opportunities and recommendations. International Journal of Advances in Scientific Research and Engineering. 5(8):53–95. doi:10.31695/IJASRE.2019.33408.

Beadel S, Shaw W, Bawden R, Bycroft C, Wilcox F, McQueen J, Lloyd K. 2018. Sustainable management of geothermal vegetation in the Waikato Region, New Zealand, including application of ecological indicators and new monitoring technology trials. Geothermics. 73:91–99. doi:10.1016/j.geothermics.2017.11.001.

Bertrand EA, Kannberg P, Caldwell TG, Heise W, Constable S, Scott B, Bannister S, Kilgour G, Bennie SL, Hart R, Palmer N. 2022. Inferring the magmatic roots of volcano-geothermal systems in the Rotorua Caldera and Okataina Volcanic Centre from magnetotelluric models. Journal of Volcanology and Geothermal Research. 431:107645. doi:10.1016/j.jvolgeores.2022.107645.

Boothroyd IKG. 2009. Ecological characteristics and management of geothermal systems of the taupo volcanic zone, New Zealand. Geothermics. 38(1):200–209. doi:10.1016/j.geothermics.2008.12.010.

Brumbaugh WG, Morman SA, May TW. 2011. Concentrations and bioaccessibility of metals in vegetation and dust near a mining Haul Road, Cape Krusenstern National Monument, Alaska. Environmental Monitoring and Assessment. 182(1–4):325–340. doi:10.1007/s10661-011-1879-z.

Bundschuh J, Maity JP. 2015. Geothermal arsenic: occurrence, mobility and environmental implications. Renewable and Sustainable Energy Reviews. 42:1214–1222. doi:10.1016/j.rser.2014.10.092.

Burns B. 1997. Vegetation change along a geothermal stress gradient at the Te Kopia steamfield. Journal of the Royal Society of New Zealand. 27(2):279–293. doi:10.1080/03014223.1997.9517539.

Calvin WM, Littlefield EF, Kratt C. 2015. Remote sensing of geothermal-related minerals for resource exploration in Nevada. Geothermics. 53:517–526. doi:10.1016/j.geothermics.2014.09.002.

Cattell HJ, Cole JW, Oze C. 2016. Volcanic and sedimentary facies of the Huka Group arc-basin sequence, Wairakei–Tauhara Geothermal Field, New Zealand. New Zealand Journal of Geology and Geophysics. 59(2):236–256. doi:10.1080/00288306.2015.1102748.

Chakraborty R, Kereszturi G, Pullanagari R, Durance P, Ashraf S, Anderson C. 2021. Mineral prospecting from biogeochemical and geological information using hyperspectral remote sensing – Feasibility and challenges. Journal of Geochemical Exploration. 232(March 2021):15. doi:10.1016/j.gexplo.2021.106900.

Ciriaco AE, Zarrouk SJ, Zakeri G. 2020. Geothermal resource and reserve assessment methodology: Overview, analysis and future directions. Renewable and Sustainable Energy Reviews. 119:109515. doi:10.1016/j.rser.2019.109515.

Deroin JP, Cochrane GR, Mongillo MA, Browne PR. 1995. Methods of remote sensing in geothermal regions: The geodynamic setting of the Taupo Volcanic Zone (North Island, New Zealand). International Journal of Remote Sensing. 16(9):1663–1677. doi:10.1080/01431169508954503.

Dunn CE. 2007. *Biogeochemical surveys at Ohui and Pine Sinter epithermal Au-Ag prospects, Coromandel, and at Waiotapu Thermal Park, New Zealand* . Lower Hutt (NZ): GNS Science. 84 p. (GNS Science report; 201 8/20). doi:10.21420/G25647.

Dunn CE, Christie AB. 2020. Tree ferns and tea trees in biogeochemical exploration for epithermal Au and Ag in New Zealand. Geochemistry: Exploration, Environment, Analysis. 20(3):299–314. doi:10.1144/geochem2019-047.

Dunn CE, Christie AB, Black J. 2018. Biogeochemical Surveys at Ohui and Pine Sinter Epithermal Au-Ag Prospects, Coromandel, and at Waiotapu Thermal Park, New Zealand. GNS Science Report 2018/20. doi:10.21420/G25647.

Elmarsdóttir Á, Vilmundardóttir OK, Magnússon SH. 2015. Vegetation of high-temperature geothermal areas in Iceland. April:19–25.

Finnegan PM, Chen W. 2012. Arsenic toxicity: the effects on plant metabolism. Frontiers in Physiology. 3 JUN (June):1–18. doi:10.3389/fphys.2012.00182.

Freski YR, Hecker C, van der Meijde M, Setianto A. 2021. The effects of alteration degree, moisture and temperature on laser return intensity for mapping geothermal manifestations. Geothermics. 97:102250. doi:10.1016/j.geothermics.2021.102250.

Gallagher A, Montanaro C, Cronin S, Scott B, Dingwell DB, Scheu B. 2020. Hydrothermal eruption dynamics reflecting vertical variations in host rock geology and geothermal alteration, Champagne Pool, Wai-o-Tapu, New Zealand. Bulletin of Volcanology. 82(12):77. doi:10.1007/s00445-020-01414-3.

Giggenbach W, Sheppard D, Robinson B, Stewart M, Lyon G. 1994. Geochemical structure and position of the Waiotapu Geothermal Field, New Zealand. Geothermics. 23(5–6):599–644. doi:10.1016/0375-6505(94)90022-1.

Giggenbach WF. 1995. Variations in the chemical and isotopic composition of fluids discharged from the Taupo Volcanic Zone, New Zealand. Journal of Volcanology and Geothermal Research. 68(95):89–116. doi:10.1016/0377-0273(95)00009-J.

Given DR. 1980. Vegetation on heated soils at Karapiti, Central North Island, New Zealand, and its relation to ground. New Zealand Journal of Botany. 18(1):1–13. doi:10.1080/0028825X.1980.10427227.

Gong J, Munoz-Saez C, Wilmeth DT, Myers KD, Homann M, Arp G, Skok JR, van Zuilen MA. 2022. Morphogenesis of digitate structures in hot spring silica sinters of the El Tatio geothermal field, Chile. Geobiology. 20(1):137–155. doi:10.1111/gbi.12471.

González-Acevedo ZI, García-Zarate MA, Núñez-Zarco EA, Anda-Martín BI. 2018. Heavy metal sources and anthropogenic enrichment in the environment around the Cerro Prieto Geothermal Field, Mexico. Geothermics. 72(May 2017):170–181. doi:10.1016/j.geothermics.2017.11.004.

Grindley G, Mumme T, Kohn B. 1994. Stratigraphy, paleomagnetism, geochronology and structure of silicic volcanic rocks, Waiotapu/Paeroa range area, New Zealand. Geothermics. 23(5–6):473–499. doi:10.1016/0375-6505(94)90014-0.

Hacıoğlu Ö, Başokur AT, Diner Ç. 2021. Geothermal potential of the eastern end of the Gediz basin, western Anatolia, Turkey revealed by three-dimensional inversion of magnetotelluric data. Geothermics. 91(May 2020). doi:10.1016/j.geothermics.2020.102040.

Hadfield J, Nicole D, Rosen M, Wilson CJL, Morgenstern U. 2001. Hydrogeology of Lake Taupo Catchment: Phase 1. In Environment Waikato Technical Report ; 2001/01.

Hamilton AR, Campbell KA, Rowland JV, Barker S, Guido D. 2019. Characteristics and variations of sinters in the Coromandel Volcanic Zone: application to epithermal exploration. New Zealand Journal of Geology and Geophysics. 62(4):531–549. doi:10.1080/00288306.2018.1519514.

Harvey M, Luketina K. 2014. Thermal infrared cameras and drones: a match made in heaven for cost- effective geothermal exploration, monitoring and development. New Zealand Geothermal Workshop 2014 Proceedings. November:1–4.

Harvey MC, Rowland JV, Luketina KM. 2016. Drone with thermal infrared camera provides high resolution georeferenced imagery of the Waikite geothermal area, New Zealand. Journal of Volcanology and Geothermal Research. 325:61–69. doi:10.1016/j.jvolgeores.2016.06.014.

Hedenquist JW. 1982. Fluid flow in the Waiotapu Geothermal System, New Zealand: implications for its potential. Proceedings of the New Zealand Geothermal Workshop. 61–67.

Hedenquist JW. 1991. Boiling and dilution in the shallow portion of the Waiotapu geothermal system, New Zealand. Geochimica et Cosmochimica Acta. 55(10):2753–2765. doi:10.1016/0016-7037(91)90442-8.

Hedenquist JW, Browne PRL. 1989. The evolution of the Waiotapu geothermal system, New Zealand, based on the chemical and isotopic composition of its fluids, minerals and rocks. Geochimica et Cosmochimica Acta. 53(9):2235–2257. doi:10.1016/0016-7037(89)90347-5.

Hegan BD, Johnson JD, Severne C. 2001. Engineering and development in hazardous terrain. Landslide risk from the Hipaua Geothermal area near Waihi Village at the southern end of Lake Taupo. New Zealand Geotechnical Society 2001 Symposium, vol. 29, 439–448.

Henley RW, Ellis AJ. 1983. Geothermal systems ancient and modern: a geochemical review. Earth-Science Reviews. 19(1):1–50. doi:10.1016/0012-8252(83)90075-2.

Jácome Paz MP, Gómez Piña VM, Prol Ledesma RM, González Romo I, Estrada Murillo A, Hernández Hernández MA, González Alfaro A, Gómez Torres M. 2021. Geoheritage in Thermal Springs of Puruándiro, Michoacán, México. Geoheritage. 13(3):68. doi:10.1007/s12371-021-00584-6.

Jácome Paz MP, Pérez-Zarate D, Prol-Ledesma RM, González Romo I, Rodríguez A. 2022. Geochemical exploration in Mesillas geothermal area, Mexico. Applied Geochemistry. 143:105376. doi:10.1016/j.apgeochem.2022.105376.

Kaya E, Hochstein MP, Yeh A, Sullivan MJO. 2015. Aspects of natural heat transfer of a geothermal system in moderate terrain: the greater Waiotapu geothermal system, New Zealand. Proceedings World Geothermal Congress 2015. April:1–12.

Kaya E, O'Sullivan MJ, Hochstein MP. 2014. A three dimensional numerical model of the Waiotapu, Waikite and Reporoa geothermal areas, New Zealand. Journal of Volcanology and Geothermal Research. 283:127–142. doi:10.1016/j.jvolgeores.2014.07.008.

Kellett RL, Bromley CJ. 2019. Geophysical signatures of New Zealand epithermal Au-Ag deposits, and methods for new exploration. New Zealand Journal of Geology and Geophysics. 62(4):442–460. doi:10.1080/00288306.2018.1548494.

Kereszturi G, Schaefer LN, Miller C, Mead S. 2020. Hydrothermal Alteration on Composite Volcanoes: Mineralogy, Hyperspectral Imaging, and Aeromagnetic Study of Mt Ruapehu, New Zealand. Geochemistry, Geophysics, Geosystems. 21(9):1–28. doi:10.1029/2020gc009270.

Lassalle G, Fabre S, Credoz A, Hédacq R, Borderies P, Bertoni G, Erudel T, Buffan-Dubau E, Dubucq D, Elger A. 2019. Detection and discrimination of various oil-contaminated soils using vegetation reflectance. Science of the Total Environment. 655:1113–1124. doi:10.1016/j.scitotenv.2018.11.314.

Lattanzi P, Benesperi R, Morelli G, Rimondi V, Ruggieri G. 2020. Biomonitoring studies in geothermal areas: a review. Frontiers in Environmental Science. 8(x):1–7. doi:10.3389/fenvs.2020.579343.

Lloyd EF. 1959. The hot springs and hydrothermal eruptions of Waiotapu. New Zealand Journal of Geology and Geophysics. 2(1):141–176. doi:10.1080/00288306.1959.10431319.

Lund JW, Freeston DH, Boyd TL. 2011. Direct utilization of geothermal energy 2010 worldwide review. Geothermics. 40(3):159–180. doi:10.1016/j.geothermics.2011.07.004.

Lund JW, Huttrer GW, Toth AN. 2022. Characteristics and trends in geothermal development and use, 1995 to 2020. Geothermics. 105:102522. doi:10.1016/j.geothermics.2022.102522.

Lynne BY. 2012. Mapping vent to distal-apron hot spring paleo-flow pathways using siliceous sinter architecture. Geothermics. 43:3–24. doi:10.1016/j.geothermics.2012.01.004.

Manzo C, Salvini R, Guastaldi E, Nicolardi V, Protano G. 2013. Reflectance spectral analyses for the assessment of environmental pollution in the geothermal site of Mt. Amiata (Italy). Atmospheric Environment. 79:650–665. doi:10.1016/j.atmosenv.2013.06.038.

Mardiati D, Setianto A, Harijoko A. 2020. Revealing geothermal potential areas with remote sensing analysis for surface temperature and lineament density: case study in south Bajawa, NTT, Indonesia. IOP Conference Series: Earth and Environmental Science. 417(1):1–16. doi:10.1088/1755-1315/417/1/012009.

Mauriohooho K, Barker SLL, Rae AJ, Simpson MP. 2014. Hydrothermal alteration of the Tauhara Geothermal Field, an active hydrothermal system. *AusIMM New Zealand Branch Annual Conference* 2014. November:371–381.

McCleskey RB, Nordstrom DK, Hurwitz S, Colman DR, Roth DA, Johnson M, Boyd ES. 2022. The source, fate, and transport of arsenic in the Yellowstone hydrothermal system – an overview. Journal of Volcanology and Geothermal Research. 432:107709. doi:10.1016/j.jvolgeores.2022.107709.

McLellan JG, Oliver NHS, Hobbs BE, Rowland JV. 2010. Modelling fluid convection stability in continental faulted rifts with applications to the Taupo Volcanic Zone, New Zealand. Journal of Volcanology and Geothermal Research. 190(1–2):109–122. doi:10.1016/j.jvolgeores.2009.11.015.

Mia MB, Bromley CJ, Fujimitsu Y. 2012. Monitoring heat flux using Landsat TM/ETM+ thermal infrared data – a case study at Karapiti ('Craters of the Moon') thermal area, New Zealand. Journal of Volcanology and Geothermal Research. 235–236:1–10. doi:10.1016/j.jvolgeores.2012.05.005.

Milicich SD, Mortimer N, Villamor P, Wilson CJN, Sagar MW, Ireland TR, Milicich SD, Mortimer N, Villamor P, Wilson CJN, et al. 2020. The Mesozoic terrane boundary beneath the Taupo Volcanic Zone, New Zealand, and potential controls on geothermal system characteristics The Mesozoic terrane boundary beneath the Taupo Volcanic Zone, New. New Zealand Journal of Geology and Geophysics. 0(0):1–12. doi:10.1080/00288306.2020.1823434.

Mongillo MA. 1994. Aerial thermal infrared mapping of the Waimangu-Waiotapu Geothermal Region, New Zealand. Geothermics. 23(5–6):511–526. doi:10.1016/0375-6505(94)90016-7.

Montanaro C, Ray L, Cronin SJ, Calibugan A, Rott S, Bardsley C, Scheu B. 2023. Linking top and subsoil types, alteration and degassing processes at Rotokawa geothermal field, New Zealand. Frontiers in Earth Science. 10:1067012. doi:10.3389/feart.2022.1067012.

Monteiro FA, Nogueirol RC, Carrijo Azevedo Melo L, Guirado Artur GA, da Rocha F. 2011. Effect of barium on growth and macronutrient nutrition in Tanzania guinea grass grown in nutrient solution. Communications in Soil Science and Plant Analysis. 42(13):1510–1521. doi:10.1080/00103624.2011.581725.

Nash GD, Moore JN, Sperry T. 2003. Vegetal-spectral anomaly detection at the Cove Fort-Sulphurdale thermal anomaly, Utah, USA: implications for use in geothermal exploration. Geothermics. 32(2):109–130. doi:10.1016/S0375-6505(03)00012-9.

Patterson JW, Driesner T, Matthai SK. 2018. Self-organizing fluid convection patterns in an en Echelon Fault Array. Geophysical Research Letters. 45(10):4799–4808. doi:10.1029/2018GL078271.

Pérez-Zárate D, Prol-Ledesma RM, Rodríguez-Díaz AA, Jácome-Paz MP, González-Romo IA. 2022. Soil gas flux, hydrogeochemistry and multicomponent geothermometry of thermal springs in the La Escalera geothermal prospect, Mexico. Applied Geochemistry. 139:105256. doi:10.1016/j.apgeochem.2022.105256.

Pippucci A, Lorenzi R, Spanò C, Sorce C. 2015. Stress-induced changes to the flora in a geothermal field in central Italy. Acta Physiologiae Plantarum. 37(10):198-1–10. doi:10.1007/s11738-015-1953-1.

Pirajno F. 2009. Hydrothermal processes and mineral systems. (Vol. 53). East Perth: Springer Netherlands. http://link.springer.com/10.1007978-1-4020-8613-7.

Pope J, Brown KL. 2014. Geochemistry of discharge at Waiotapu geothermal area, New Zealand – Trace elements and temporal changes. Geothermics. 51:253–269. doi:10.1016/j.geothermics.2014.01.006.

Pullagurala VLR, Rawat S, Adisa IO, Hernandez-Viezcas JA, Peralta-Videa JR, Gardea-Torresdey JL. 2018. Plant uptake and translocation of contaminants of emerging concern in soil. Science of The Total Environment. 636:1585–1596. doi:10.1016/j.scitotenv.2018.04.375.

Pullanagari RR, Kereszturi G, Yule IJ. 2016. Mapping of macro and micro nutrients of mixed pastures using airborne AisaFENIX hyperspectral imagery. ISPRS Journal of Photogrammetry and Remote Sensing. 117:1–10. doi:10.1016/j.isprsjprs.2016.03.010.

Qudsi I, Noor MR. 2022. Geothermal surface manifestation identification using airborne hyperspectral imagery case study: Davis-Schrimpf Geothermal Field, Salton Sea, California. Indonesian Journal on Geoscience. 9(1):119–130. doi:10.17014/ijog.9.1.119-130.

Rathod PH, Brackhage C, Müller I, Van der Meer FD, Noomen MF. 2018. Assessing metal-induced changes in the visible and near-infrared spectral reflectance of leaves: a pot study with sunflower (Helianthus annuus L.). Journal of the Indian Society of Remote Sensing. 3(3):1–13. doi:10.1007/s12524-018-0846-3.

Rattenbury M, Martin A, Baisden T, Turnbull R, Rogers K. 2018. Geochemical baseline soil surveys for understanding element and isotope variation across New Zealand. New Zealand Journal of Agricultural Research. 61(3):347–357. doi:10.1080/00288233.2018.1426616.

Reeves R, Sanders F. 2019. 2019 thermal infrared survey of the Waiotapu Geothermal Field. (p. 29). Wairakei (NZ): GNS Science (GNS Science report; 2019/57). doi:10.21420/ZD6D-GD88.

Renewable Energy Agency, I., & Geothermal Association, I. 2021. United Nations Framework Classification for Geothermal Energy: Pilot applications in the Caribbean, Ethiopia and Indonesia. www.irena.org.

Rodriguez-Gomez C, Kereszturi G, Jeyakumar P, Pullanagari R, Reeves R, Rae A, Procter JN. 2023a. Remote exploration and monitoring of geothermal sources: a novel method for foliar element mapping using hyperspectral (VNIR-SWIR) remote sensing. Geothermics. 111:102716. doi:10.1016/j.geothermics.2023.102716.

Rodriguez-Gomez C, Kereszturi G, Reeves R, Rae A, Pullanagari R, Jeyakumar P, Procter JN. 2021. Lithological mapping of Waiotapu Geothermal Field (New Zealand) using hyperspectral and thermal remote sensing and ground exploration techniques. Geothermics. 96(June):102195. doi:10.1016/j.geothermics.2021.102195.

Rodriguez-Gomez C, Kereszturi G, Whitehead M, Reeves R, Rae A, Pullanagari R. 2023b. Point pattern analysis of thermal anomalies in geothermal fields and its use for inferring shallow hydrological processes. Geothermics. 110:102664. doi:10.1016/j.geothermics.2023.102664.

Rowland JV, Sibson RH. 2004. Structural controls on hydrothermal flow in a segmented rift system, Taupo Volcanic Zone, New Zealand. Geofluids. 4(4):259–283. doi:10.1111/j.1468-8123.2004.00091.x.

Rowland JV, Simmons SF. 2012. Hydrologic, magmatic, and tectonic controls on hydrothermal flow, Taupo Volcanic Zone, New Zealand: implications for the formation of epithermal vein deposits. Economic Geology. 107(3):427–457. doi:10.2113/econgeo.107.3.427.

Sanches ID, Souza Filho CR, Magalhães LA, Quitério GCM, Alves MN, Oliveira WJ. 2013. Unravelling remote sensing signatures of plants contaminated with gasoline and diesel: an approach using the red edge spectral feature. Environmental Pollution. 174:16–27. doi:10.1016/j.envpol.2012.10.029.

Santaga FS, Agnelli A, Leccese A, Vizzari M. 2021. Using Sentinel-2 for simplifying soil sampling and mapping:

two case studies in Umbria, Italy. Remote Sensing. 13 (17):3379. doi:10.3390/rs13173379.

Seebeck H, Nicol A, Villamor P, Ristau J, Pettinga J. 2014. Structure and kinematics of the Taupo Rift, New Zealand. Tectonics. 33(6):1178–1199. doi:10.1002/2014TC003569.

Seward A, Reeves R, Alcaraz S. 2022. Assessment of the surface heat loss from Waimangu Geothermal Valley: Comparison of terrestrial based assessment techniques with remote sensing. Journal of Volcanology and Geothermal Research. 430(July):107630. doi:10.1016/j.jvolgeores.2022.107630.

Simpson MP, Bignall G. 2016. Undeveloped high-enthalpy geothermal fields of the Taupo Volcanic Zone, New Zealand. Geothermics. 59:325–346. doi:10.1016/j.geothermics.2015.08.006.

Simpson MP, Christie AB. 2019. Hydrothermal alteration mineralogical footprints for New Zealand epithermal Au-Ag deposits. New Zealand Journal of Geology and Geophysics. 62(4):483–512. doi:10.1080/00288306.2019.1577278.

Sleimi N, Kouki R, Hadj Ammar M, Ferreira R, Pérez-Clemente R. 2021. Barium effect on germination, plant growth, and antioxidant enzymes in Cucumis sativus L. plants. Food Science and Nutrition. 9(4):2086–2094. doi:10.1002/fsn3.2177.

Slonecker T, Haack B, Price S. 2009. Spectroscopic analysis of arsenic uptake in Pteris ferns. Remote Sensing. 1 (4):644–675. doi:10.3390/rs1040644.

Smale MC, Fitzgerald NB. 2015. Geothermal vegetation types of the Taupō Volcanic Zone (Vol. 4355). Hamilton: Waikato Regional Council.

Smale MC, Wiser SK, Bergin MJ, Fitzgerald NB. 2018. A classification of the geothermal vegetation of the Taupō Volcanic Zone, New Zealand. Journal of the Royal Society of New Zealand. 48(1):21–38. doi:10.1080/03036758.2017.1322619.

Soltani M, Kashkooli FM, Dehghani-Sanij AR, Kazemi AR, Bordbar N, Farshchi MJ, Elmi M, Gharali K, Dusseault MB. 2019. A comprehensive study of geothermal heating and cooling systems. Sustainable Cities and Society. 44:793–818. doi:10.1016/j.scs.2018.09.036.

Steiner A. 1963. The rocks penetrated by drillholes in the Waiotapu thermal area, and their hydrothermal alteration. In Waiotapu Geothermal Field. New Zealand Department of Scientific and Industrial Research Bulletin. 155:26–35.

Suherlina L, Newson J, Kamah Y, Brehme M. 2022. The dynamic evolution of the Lahendong geothermal system in North-Sulawesi, Indonesia. Geothermics. 105:102510. doi:10.1016/j.geothermics.2022.102510.

Sun J, Liu K, He Q, Yu T, Deng Y. 2022. Thermal infrared remote sensing and soil gas radon for detecting blind geothermal area. Geothermics. 105:102534. doi:10.1016/j.geothermics.2022.102534.

Tschan M, Robinson BH, Schulin R. 2009. Antimony in the soil – Plant system – a review. Environmental Chemistry. 6(2):106–115. doi:10.1071/EN08111.

Ünal Ercan H, Işık Ece Ö, Schroeder PA, Gülmez F. 2022. Characteristics and evolution of the Etili silica sinter epithermal deposits, Çanakkale – Turkey: Relation to alkali chloride vs acid-sulfate fluids. Ore Geology Reviews. 142:104726. doi:10.1016/j.oregeorev.2022.104726.

Van Manen SM, Reeves R. 2012. An assessment of changes in kunzea ericoides var. Microflora and other hydrothermal vegetation at the Wairakei-Tauhara geothermal field, New Zealand. Environmental Management. 50(4):766–786. doi:10.1007/s00267-012-9899-1.

Wang F, Gao J, Zha Y. 2018. Hyperspectral sensing of heavy metals in soil and vegetation: feasibility and challenges. ISPRS Journal of Photogrammetry and Remote Sensing. 136:73–84. doi:10.1016/j.isprsjprs.2017.12.003.

Way W, Hall S. 2001. Cost-effective vegetation anomaly mapping for geotherma exploration. Proceedings: Twenty-Sixth Workshop on Geothermal Reservoir Engineering. Stanford University, Stanford, California, January 29–30, 2001 SGP-TR-168, 2.

Wei Z-A, Shao H, Tang L, Deng B, Li H, Wang C. 2021. Hydrogeochemistry and geothermometry of geothermal waters from the Pearl River Delta region, South China. Geothermics. 96:102164. doi:10.1016/j.geothermics.2021.102164.

White NC, Hedenquist JW. 1990. Epithermal environments and styles of mineralization: variations and their causes, and guidelines for exploration. Journal of Geochemical Exploration. 36(1–3):445–474. doi:10.1016/0375-6742(90)90063-G.

Wilson CJN, Rowland JV. 2016. The volcanic, magmatic and tectonic setting of the Taupo Volcanic Zone, New Zealand, reviewed from a geothermal perspective. Geothermics. 59:168–187. doi:10.1016/j.geothermics.2015.06.013.

Wilson SC, Lockwood PV, Ashley PM, Tighe M. 2010. The chemistry and behaviour of antimony in the soil environment with comparisons to arsenic: a critical review. Environmental Pollution. 158(5):1169–1181. doi:10.1016/j.envpol.2009.10.045.

Wood CP. 1994. Aspects of the geology of Waimangu, Waiotapu, Waikite and Reporoa geothermal systems, Taupo Volcanic Zone, New Zealand. Geothermics. 23 (5–6):401–421. doi:10.1016/0375-6505(94)90011-6.

Zaini N, Yanis M, Abdullah F, Van Der Meer F, Aufaristama M. 2022. Exploring the geothermal potential of Peut Sagoe volcano using Landsat 8 OLI/TIRS images. Geothermics. 105(November 2021):102499. doi:10.1016/j.geothermics.2022.102499.

Zhou C. 2021. Near-Surface Geothermal Reservoir Imaging based on the Customized Dense Seismic Network. Surveys in Geophysics. 42:673–697.